Second Order Jahn-Teller Interactions at Unusually High Molecular Orbital Energy Separations

Journal:	*Dalton Transactions*
Manuscript ID	DT-ART-01-2020-000137.R1
Article Type:	Paper
Date Submitted by the Author:	14-Mar-2020
Complete List of Authors:	Wedler, Henry; University of California, Davis, Chemistry Wendelboe, Paul; University of California, Davis, Chemistry Tantillo, Dean; University of California, Davis, Chemistry; Power, Philip; University of California, Department of Chemistry

Second Order Jahn-Teller Interactions at Unusually High Molecular Orbital Energy Separations

Henry B. Wedler,[⊗] Paul Wendelboe,[⊗] Dean J. Tantillo* and Philip P. Power*

Department of Chemistry, University of California–Davis, Davis, CA USA

[⊗] These authors contributed equally.

* pppower@ucdavis.edu

Abstract

Second order Jahn-Teller (SOJT) effects arise from interactions between filled and empty molecular orbitals of like symmetry. These interactions often lead to structural distortions whose extent is inversely proportional to the energy difference between the interacting orbitals. The main objectives of the work described here are (1) the calculation (using density functional theory methods) of the energies of the valence molecular orbitals in the species EH_3 (E = N, P, As or Sb), HEEH (E = C, Si, Ge or Sn), and H_2EEH_2, (E = C, Si, Ge or Sn) and (2) the correlation of these energies with barriers for planarization or linearization. The calculations suggest an upper limit of about 12 eV energy separation of the interacting levels for SOJT effects to be significant, which is considerably larger than previously thought and implies that SOJT effects may be more common than currently realized.

Introduction

The process by which pyramidal molecules of the general formula ER_3 (E=N–Bi; R=H, alkyl, aryl, silyl, halide, etc., or the corresponding anionic group 14 and cationic group 16 species) are transformed into their inverted conformation (Figure 1) has been studied both experimentally[1] and theoretically[2-8] for many decades. A detailed understanding of this process is of fundamental interest with respect to bonding in these molecules and chemical bonding in general. Classically, the inversion process can be regarded as a (fundamental) vibrational mode that interconverts the two pyramidal conformations via a planar transition state structure.[9] The energy difference between the pyramidal minimum and the transition state structure is the so-called inversion barrier. The magnitude of the inversion barrier is related to several factors.[1] These include the relative electronegativity (EN) of the substituents (R) and central atom (E), conjugative interactions between E and R, the steric properties of R, the presence of lone pairs on R and geometrical constraints at E. The influence of electronic factors, e.g., the EN values of the central and substituent atoms, has been rationalized in terms of the Bent[11]/Walsh[12,13] rules and differences in hybridization tendencies between the lightest and heavier elements within each group (Kutzelnigg).[14] Conjugation can lower the relative energy of the planar transition state structure and geometrical confinement can increase the relative strain of the minimum or transition state structure.[15]

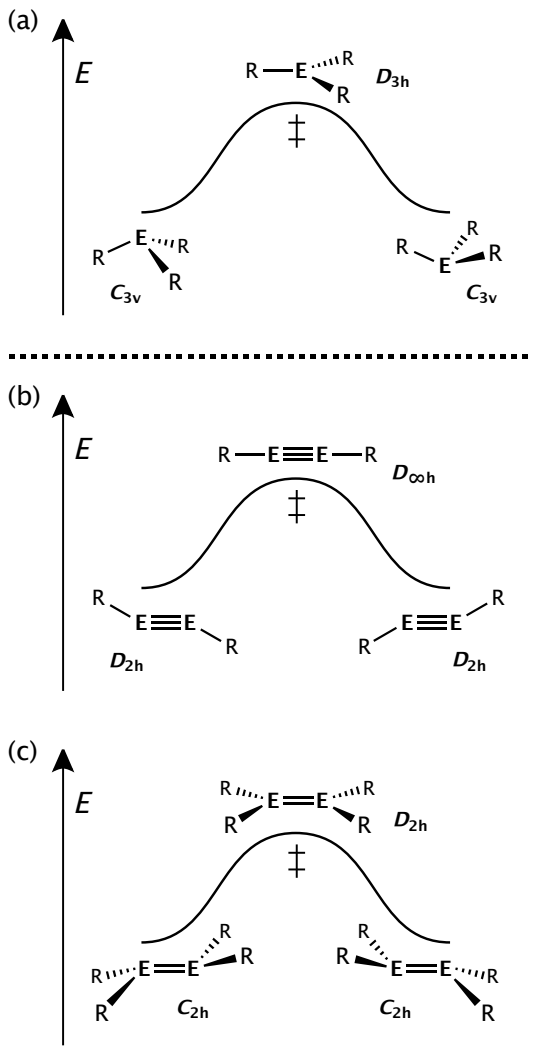

Figure 1. Inversion/linearization processes examined herein.

A less prominent view of the inversion process is based on second order Jahn-Teller (SOJT) effects[16-23] involving the extent of HOMO-LUMO interactions and their dependence on symmetries of the frontier orbitals and the electronegativities of E and R. These effects are ubiquitous in chemistry, and in molecular species they generally involve a symmetry governed interaction between a filled and an empty molecular orbital that occurs during a molecular vibration. This interaction can produce a change in the geometry that usually far exceeds those produced by the better known but arguably less important (for chemistry) first order Jahn-Teller effect. The extent of the SOJT distortion is inversely proportional to the

energy difference between the interacting levels. It was pointed out recently that there was no information available on the energy separations between the levels whose interactions produced the SOJT distortion,[26] and it is generally thought that for SOJT effects to be observable there is an upper limit of ca. 4 eV in the energy separation of the levels.[17,18]

The relative energies of the frontier orbitals for the structures in Figure 1 are reflected in the magnitude of the inversion barrier, yet relatively few calculations[8] that provide energies of the symmetrically relevant interacting frontier orbitals for a series of ER_3 species with varying E or R groups have been published to date.[24] Inversion or linearization processes for pyramidal or bent geometries found for the heavier main group element analogues of alkenes and alkynes are closely related to the ER_3 inversion process (Figure 1b,c),[19-21] and theoretical studies that relate these processes to SOJT effects are also scarce.[25,26]

Here we describe the results of calculations on the trigonal pyramidal hydrides of group 15 atoms with emphasis on the relative energies of frontier orbitals and their implications for inversion barriers. We also describe parallel calculations on the group 14 heavier element ethene and ethyne analogues, which possess trans-pyramidalized (folded) or trans-bent structures in contrast to their planar or linear carbon analogues (Figure 1b,c).[27] We emphasize the symmetries and energies of the frontier orbitals during the inversion or linearization process and show that SOJT interactions occur even when HOMO-LUMO energy separations are as high as 12 eV, much higher than the previous estimate of 4 eV.[28]

Methods

All computations were performed using the *Gaussian09* software suite.[29] Calculations were performed with the ωB97X-D functional and the Def2-TZVPP basis set.[30] All calculations utilized an

ultrafine quadrature grid (implemented using the "int=ultrafine" command). Some calculations were carried out at the coupled cluster singles and doubles with perturbative triples (CCSD(T)) level,[31] with the aug-cc-pVQZ basis set.[32] The results of these calculations, which confirmed, for NH_3 and PH_3, that the ωB97X-D/Def2-TZVPP model chemistry satisfactorily predicted orbital energies, are described in the Supporting Information. *CylView*,[33] and *Avogadro*[34] were used to generate ball-and-stick and orbital (isovalue of 0.02000) images, respectively. To generate molecular orbital diagrams, a custom python script utilizing *matplotlib* was employed.[35]

For the pnictogens, the calculated pyramidal geometries for all equilibrium structures feature C_{3v} point group symmetry. In our case, where R=H, all pnictogen transition state structures have D_{3h} symmetry. Nevertheless, recent calculations by Truhlar and coworkers have shown that when the substituent is a halogen and E is a heavier pnictogen (e.g., P-Bi), the transition state structures can be T-shaped with C_{2v} symmetry.[9] In addition, open-shell species can also participate in inversion.[9] However, we focus here on the closed shell $C_{3v} \rightleftharpoons D_{3h} \rightleftharpoons C_{3v}$ process and the related processes in HEEH and H_2EEH_2.

Results and Discussion

ER_3 Systems

A symmetry-directed approach to relate inversion and trans-bending barriers with the relative energies of the interacting molecular orbitals was used. First, we tested our computational approach by calculating molecular geometries, energies of valence orbitals, and inversion barriers for simple EH_3 (E = N, P, As and Sb) molecules.[36] The trigonal pyramidal minimum geometries have C_{3V} symmetry and the planar transition state structures have D_{3h} symmetry. In the D_{3h} structures, the HOMO-2, HOMO-1, HOMO, LUMO, and LUMO+1 orbitals have the symmetries a_1', e', a_2'', a_1', and e', respectively (Table 1 and Figure

2). Shown in Figure 2 is a representation of each molecular orbital for EH_3 corresponding to the above-named MO symmetries. This sequence, which is in order of increasing energy, is observed in the four EH_3 molecules of the group. The energy spread of the highest and lowest energy levels reflects the E–H bond strengths, and ranges from 30.62 eV in NH_3 to 20.96 eV in SbH_3. The computed HOMO-LUMO energy separation for planar, D_{3h} NH_3 (11.85 eV) is higher by >2 eV than those of its heavier congeners PH_3 (9.73 eV), AsH_3 (8.83 eV) and SbH_3 (7.51 eV). Thus, when the undistorted, planar D_{3h} NH_3 molecule undergoes a pyramidalization vibration of a_2'' symmetry, the triple direct product of the HOMO x vibration x LUMO (i.e., a_2''x a_2''x a_1' = a_1') is the totally symmetric irreducible representation of the point group D_{3h}. In other words, the mixing becomes symmetry-allowed upon the vibrational distortion from D_{3h} to C_{3V} and, in this case, it produces a stabilization of the HOMO (lone pair) that correlates to the inversion barrier. Due to the larger HOMO-LUMO energy difference in NH_3 in comparison to those of its heavier congeners, the interaction between these orbitals is relatively small and produces a low inversion barrier near 0.18 eV (4.2 kcal/mol). In other words, since the energy gap in planarized ammonia compared to its heavier congeners is large, there is less mixing and a smaller interaction between the two levels. In contrast, for the heavier congeners with smaller HOMO-LUMO energy differences, the HOMO-LUMO interaction is greater and affords much higher inversion barriers in the range 1.43 to 1.98 eV (33.0 to 45.7 kcal/mol). The calculated HOMO-LUMO energy differences mirror, but are slightly larger than, those reported earlier by Schwertfeger, Laakkonen and Pyykkö; in addition, we calculate substantially larger energy differences (ca. 1.2-2.1 eV) between the unoccupied LUMO and LUMO+1 levels (Table S1) than those (ca. 0.2 eV) calculated earlier.[8] Figure 3 shows that computed inversion barriers and orbital energy gaps correlate (R^2 = 0.95).

Table 1. The predicted energy differences between the interacting a_2`` HOMO and the a_1` LUMO in the D_{3h} planar, geometry EH_3 systems and predicted barriers for inversion.

Molecule	***ΔE (eV)***	***Inversion Barrier (kcal/mol)***
NH_3	11.85	4.2
PH_3	9.73	33.0
AsH_3	8.83	39.0
SbH_3	7.51	45.7

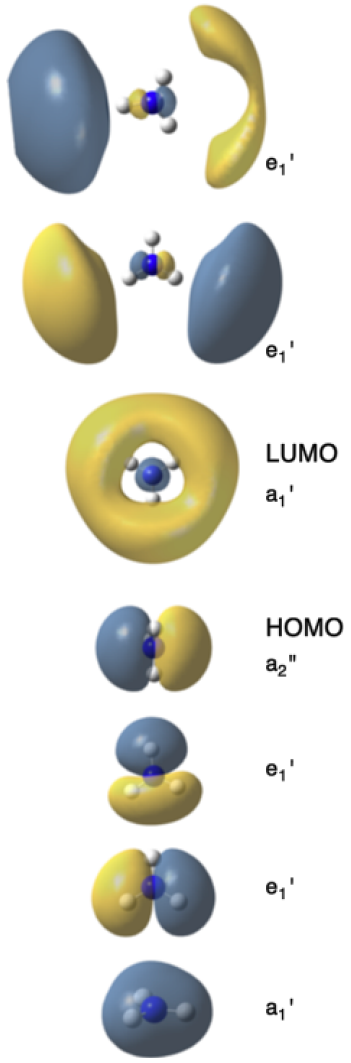

Figure 2. Representations of the computed molecular orbitals of ammonia in D_{3h} symmetry. Note that different molecular orientations are used for different orbitals to facilitate comprehension of orbital shapes.

1

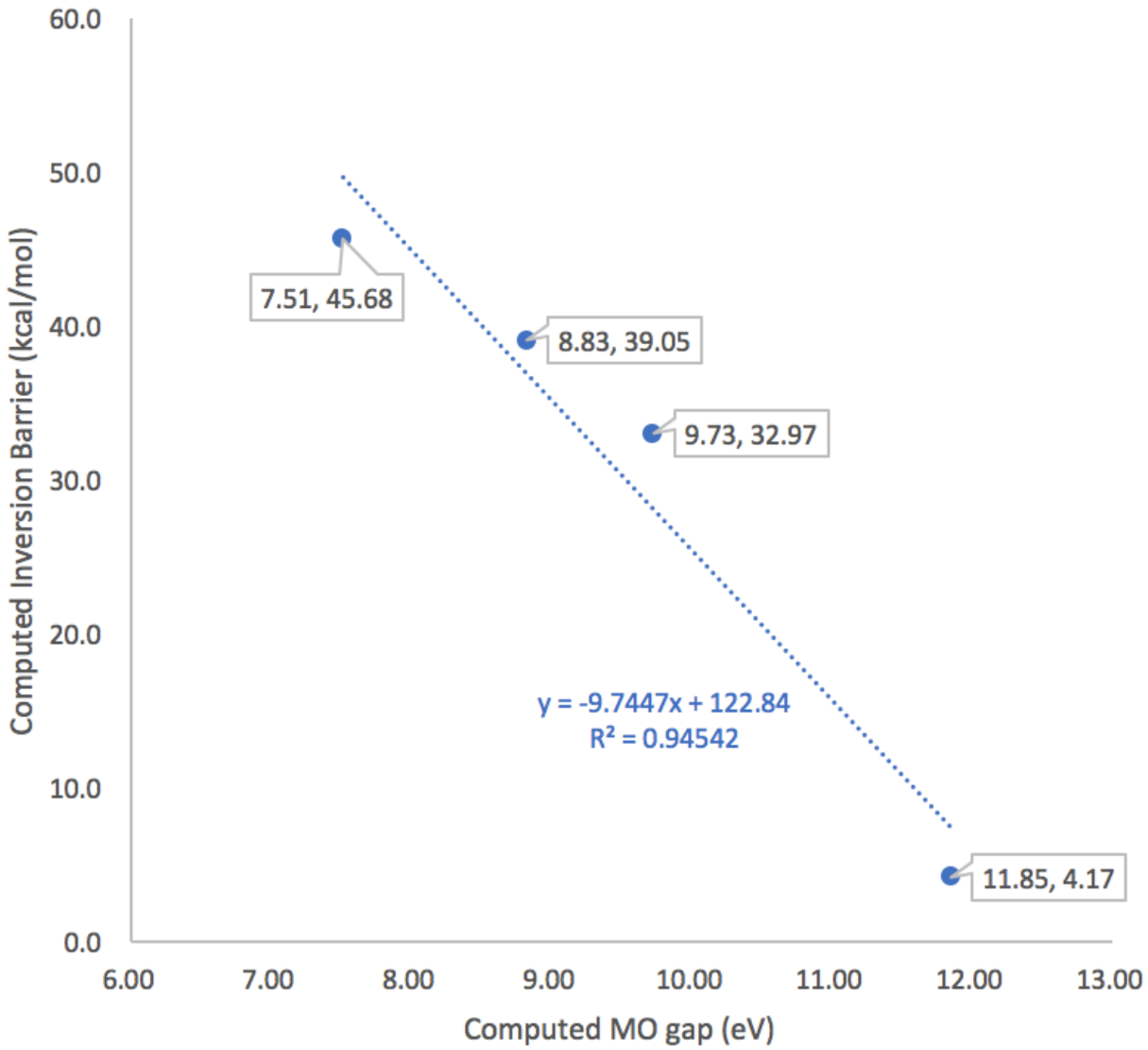

2

3 **Figure 3.** Correlation between computed inversion barrier and computed energy gap between the
4 interacting occupied and unoccupied MOs of a_1 symmetry in EH_3 molecules.

5

6 In pyramidal ammonia with C_{3v} symmetry, the valence orbitals have the symmetries $a_{1,}$ e, a_1, a_1,
7 and e, in order of increasing energy. This order parallels the sequence given above for NH_3 in D_{3h} symmetry
8 (Figures 2 and 4). The energy range of the highest and lowest molecular orbital energy levels is 31.02 eV

which is just 0.40 eV greater than that of the D_{3h} structure. In contrast, for the heavier PH_3, AsH_3, and SbH_3 analogues in C_{3v} symmetry, the ordering of the two highest energy levels changes so that the sequence becomes a_1, e, a_1, e, a_1. However, the energy differences between the highest e and a_1 levels are relatively low: 0.34 eV (PH_3), 0.22 eV (AsH_3) and 1.02 eV (SbH_3), compared to 2.3 eV in NH_3. Nonetheless, we regard the reversal of the order of the two highest energy orbitals as a consequence of the SOJT mixing of the HOMO and LUMO (a_2'' and a_1' in D_{3h} symmetry), which produces two a_1 levels in C_{3v} symmetry one of which (the HOMO) is stabilized. These changes in energy are sufficiently small in NH_3 that the ordering of the orbitals remains unchanged. In contrast, in the heavier PH_3, AsH_3 and SbH_3, the SOJT interactions are significantly larger and the energy of the LUMO is increased sufficiently to become the LUMO+2 level for the C_{3v} geometry. Other considerations such as changing orbital overlap and bond strengths can affect the ordering, but the increased SOJT interactions in the heavier element derivatives offer a simple and straightforward model for the changed ordering.

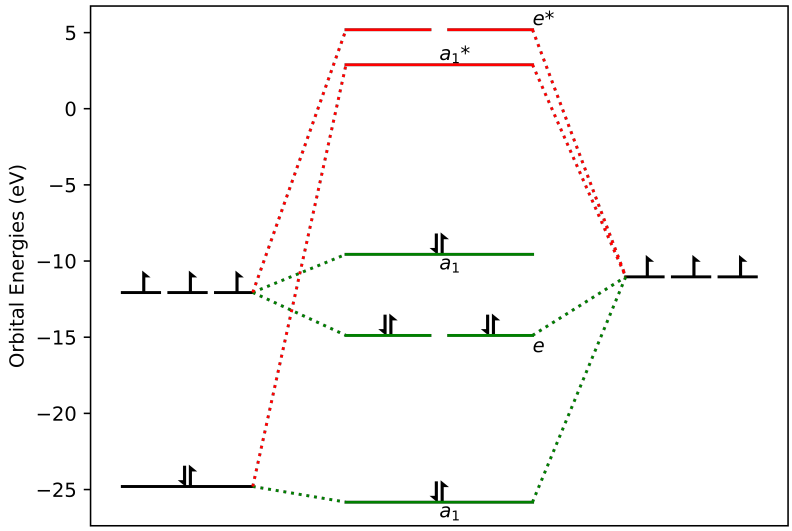

(a)

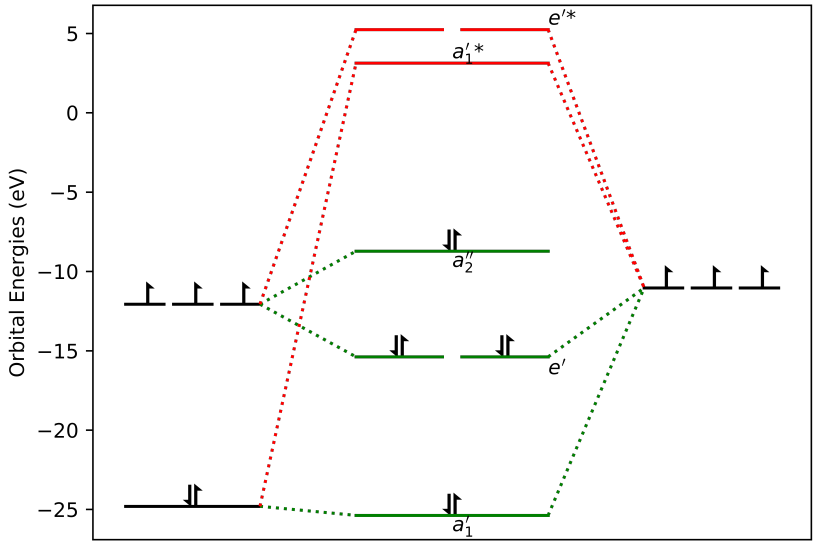

(b)

Figure 4. Molecular orbital diagram for NH_3 in (a) C_{3v} symmetry and (b) D_{3h} symmetry. The ordering of the upper two energy levels is reversed for E = P, As and Sb.

REER and R_2EER_2 Molecules

The bonding in the undistorted linear and planar HEEH alkyne and H_2EEH_2 alkene and their heavier congeners (E = C, Si, Ge or Sn), respectively was also investigated.[37] For the silicon, germanium and tin alkyne analogues, the lowest energy (non-hydrogen bridged) structure was found to have a planar, trans-bent geometry with C_{2h} symmetry (Figure 1b; Table 2). In the case of carbon, the lowest energy structure was calculated to be linear ($D_{\infty h}$), as expected. For the alkene analogues, carbon has the expected planar geometry with D_{2h} symmetry, whereas the trans-bent geometries with C_{2h} symmetry (Figure 1c) were predicted for the heavier element structures. Shown in Figure 5 is a representation of each molecular orbital for representative heavier element alkyne and alkene analogues corresponding to their respective MOs.

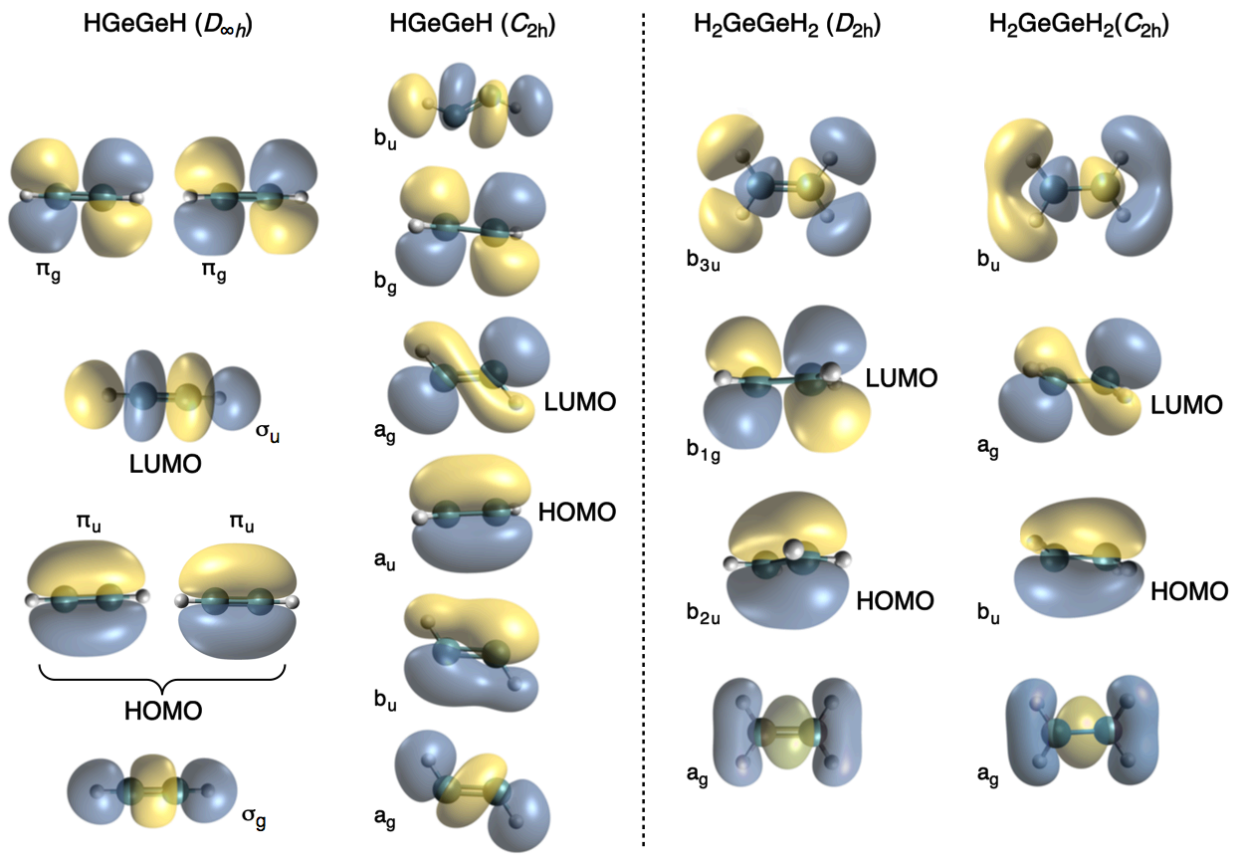

Figure 5. Orbital illustrations. Left to right: HGeGeH in $D_{\infty h}$ symmetry, HGeGeH in C_{2h} symmetry, H_2GeGeH_2 in D_{2h} symmetry, and H_2GeGeH_2 in C_{2h} symmetry, with illustrations of the calculated orbitals. Note that different molecular orientations are used for different orbitals to facilitate comprehension of orbital shapes.

Table 2. The predicted energy differences between the interacting π_u HOMO and the σ_u LUMO, which lead to a SOJT interaction upon undergoing a trans-bending vibration of C_{2h} symmetry, and predicted barriers for inversion.

Molecule	***ΔE (eV)***	***Linearization Barrier (kcal/mol)***
HCCH	14.13	0.0
HSiSiH	7.71	20.2
HGeGeH	7.16	29.5
HSnSnH	5.82	48.9

In the case of ethyne, HCCH, we start with the $D_{\infty h}$ point group (linear geometry) where we defined the HOMO-1, HOMO, LUMO and LUMO+1 as σ_g, π_u (doubly degenerate), π_g (doubly degenerate) and σ_u levels. However, in the heavier Si, Ge and Sn alkyne analogues,[37] in $D_{\infty h}$ linear geometry, we find the sequence of orbital energies has changed to σ_g, π_u (doubly degenerate), σ_u and π_g (doubly degenerate) (Figure 6). This is due to the large increase in electronic repulsion generated by the heavier cores, especially for the valence s electrons.[38] The π_u and π_g orbitals are doubly degenerate in the linear geometry, whereas, in the planar trans-bent geometry of C_{2h} symmetry, the degeneracy of the π-orbitals is lifted and one of the original π-orbitals (the in-plane π-orbital) becomes an orbital of b_u symmetry (the out of plane π-orbital has a_u symmetry) in the trans-bent species with non-bonding character as a result of its interaction with a σ* orbital. In the C_{2h} structure the energy levels corresponding to HOMO-2, HOMO-1, HOMO, LUMO, LUMO+1, and LUMO+2 levels have the symmetries a_g, b_u, a_u, a_g, b_g, b_u respectively. This order holds for all studied alkyne analogues in C_{2h} trans-bent geometry.

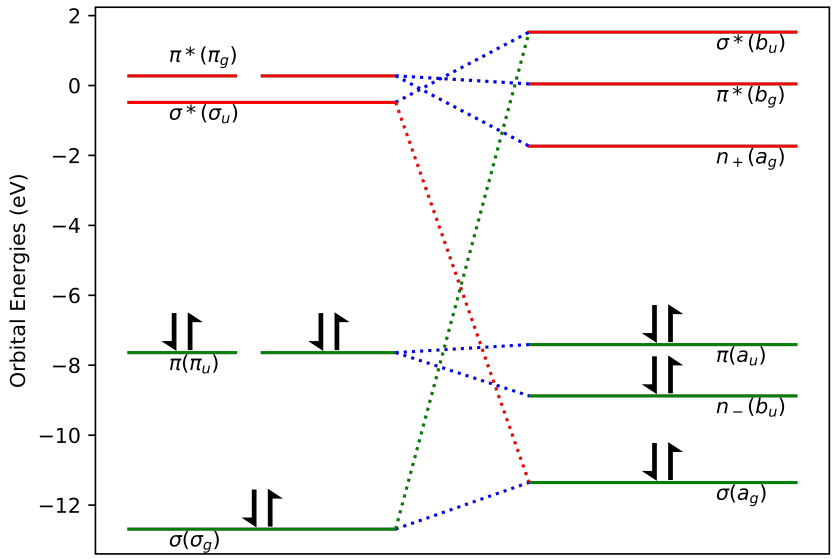

Figure 6. Correlation of the interacting valence orbitals of HGeGeH in linear $D_{\infty h}$ (left) and trans-bent C_{2h} (right) geometries.

For linear HCCH in $D_{\infty h}$ symmetry, LUMO and LUMO+1 are the antibonding π_g* and σ_u* orbitals. In the corresponding heavier element Si, Ge and Sn species in $D_{\infty h}$ symmetry, this ordering is changed (see above) and the LUMO becomes the σ_u* orbital and the LUMO+1 becomes the π_g* orbital. Upon trans-bending, the σ_u* orbital becomes b_u in C_{2h} symmetry and one of the original π-bonding orbitals also becomes b_u in symmetry. Thus, as the energy separations between the orbitals decrease in the heavier element species, the interaction between the two b_u orbitals increases and non-bonded electron density is generated at the group 14 atom, which favors the trans-bent geometry due to electron/electron repulsion.

We note that for alkene analogues, the ordering of the orbitals upon changing from E=C to heavier elements is far less important than in the case of alkyne analogues (Figure 7). While we see changes in relative MO energies as we move through the alkene analogues, the changes mainly involve orbitals that

are lower in energy than the HOMO, in contrast to the alkyne analogues where all energy differences mentioned involve orbitals that are very close to those involved in the interactions with which we are concerned here. While the HOMO is the interacting b_{3u} orbital for all the alkene analogues, we can see that the interacting unoccupied MO b_{1u}, is not the LUMO or LUMO+1 until we get to E=Ge and Sn. For E=Si, it is, in terms of energy, at the LUMO+2 level and for E=C, it is all the way at the LUMO+3 level. This also is reflected in the fact that while there is a trans-pyramidalization in the E=Si molecule, it is much smaller than the corresponding bends for E=Ge and Sn (Table 3).

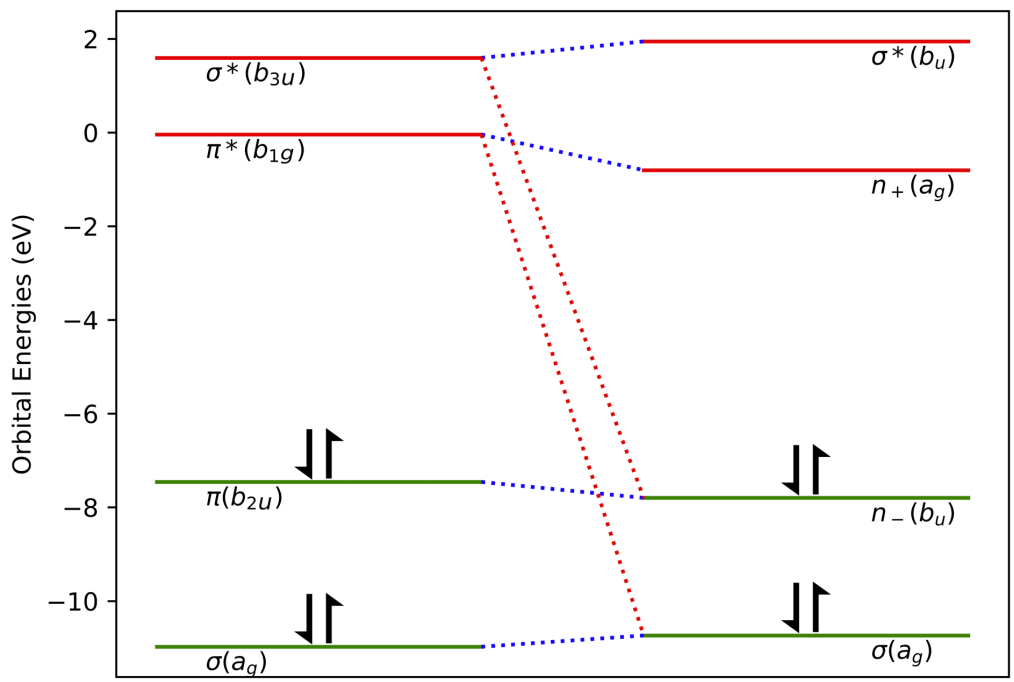

Figure 7. Comparison and correlation of D_{2h} (left) and C_{2h} (right) symmetries for H_2GeGeH_2.

Table 3. The interacting molecular orbitals (b_{2u} HOMOs and b_{3u} LUMOs) and their energies in the alkene analogues. Inversion barriers are in kcal mol^{-1}.

Molecule	***ΔE (eV)***	***Planarization Barrier (kcal/mol)***
H_2CCH_2	14.54	0.0
H_2SiSiH_2	9.78	0.9
H_2GeGeH_2	9.05	2.7
H_2SnSnH_2	7.44	10.1

Again, correlations between orbital energy gap and inversion barriers are observed for both alkene and alkyne analogues (Figures 8 and 9).

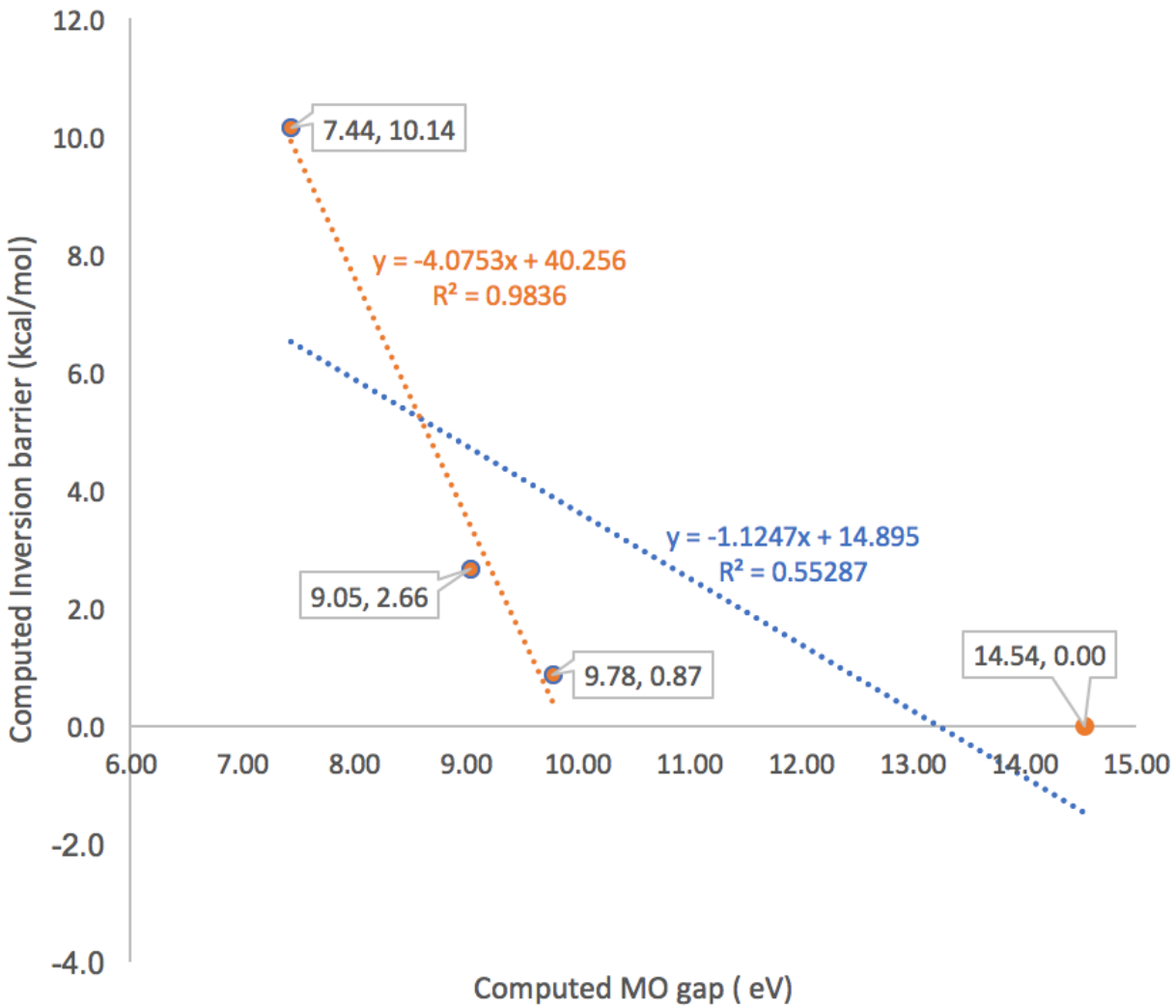

Figure 8. Plot of the planarization barriers against the energy separation of the two interacting (occupied and unoccupied) MOs for ethylene and its heavier element congeners. Using a best fit line, an R^2 value of 0.5529 is calculated. When carbon is excluded, an R^2 value of 0.9936 is calculated.

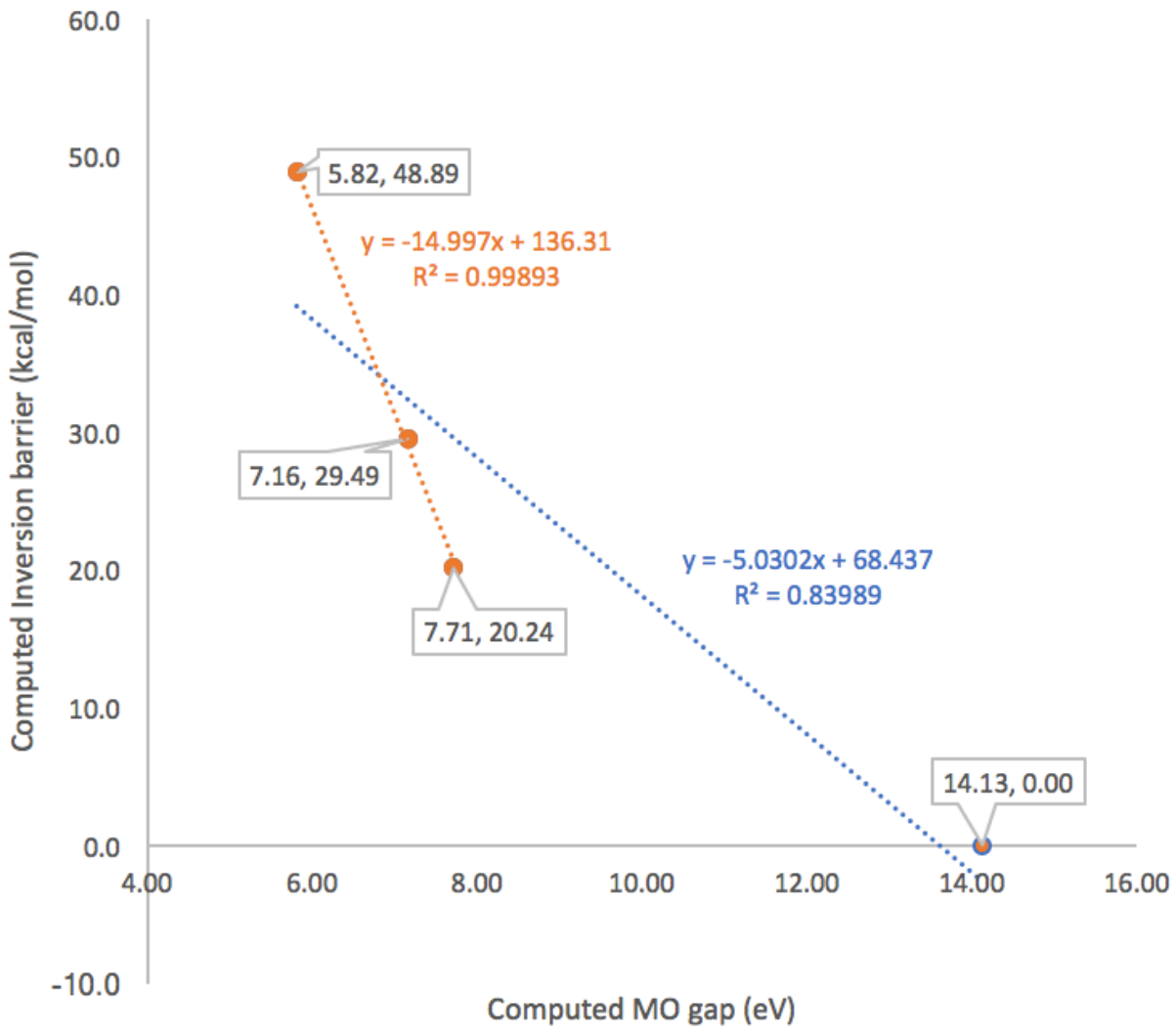

Figure 9. Plot of the linearization barriers in HEEH (E = C, Si, Ge or Sn) against the two interacting occupied and unoccupied MOs. Using a best-fit line, an R^2 value of 0.8399 is calculated. But when carbon is omitted, an R^2 value of 0.9989 is computed.

Conclusions

Here we examined the relationship between SOJT interactions and planarization/linearization barriers. For the EH_3, HEEH, and H_2EEH_2 species that we examined, SOJT interactions are important even when the energy difference between HOMO and the relevant interacting unoccupied orbital is as large as

ca. 12 eV, a much larger value than expected. For carbon-containing compounds HCCH, and H_2CCH_2, the predicted occupied/unoccupied orbital energy differences are >14 eV and no SOJT effects are apparent. In contrast, for the heavier element silicon, germanium, and tin analogues the energy differences tend to range from 5-10 eV, and these energies are sufficiently low that orbital interactions lead to the experimentally observed geometrical distortions, which, in some cases, lead to dissociation of the EE bond.[39] The unexpectedly high magnitude of the energy separations found here implies that SOJT effects of this type could be much more common than is currently realized.

Acknowledgements

We gratefully acknowledge computational support from NSF's XSEDE program. PPP thanks NSF (CHE-1565501) for financial support. HBW gratefully acknowledges Sarah Cohen for helpful feedback, assistance, and advice while performing this work.

References

(1) Rauk, A.; Allen, L. C.; Mislow, K. Pyramidal Inversion. *Angew. Chem. Int. Ed.* **1970**, *9*, 400-414.

(2) Swalen, J. D.; Ibers, J. A. Potential Function for the Inversion of Ammonia. *J. Chem. Phys.* **1962**, *36*, 1914-1918.

(3) Koeppl, G. W; Sagatys, D. S., Krishnamurthy, G. S.; Miller, S. I. Inversion Barriers of Pyramidal (XY_3) and Related Planar (=XY) Species. *J. Am. Chem. Soc.* **1967**, *89*, 3396-3425.

(4) Lehn, J. M.; Munsch, B. Electronic Structure and Inversion Barrier of Phosphine. An Ab Initio SCF–LCAO–MO Study. *Chem. Commun.* **1969**, 1327-1329.

(5) Baechler, R. D.; Mislow, K. Effect of Ligand Electronegativity on the Inversion Barrier of Phosphines. *J. Am. Chem. Soc.* **1971**, *93*, 773-774.

(6) Marynck, D. S. The inversion barriers of NF_3, NCl_3, PF_3 and PCl_3. A theoretical study. *J. Chem. Phys.* **1980**, *73*, 3939-3943.

(7) Boldyrev, A. I.; Charkin, O. P. Inversion of Pyramidal and Tetrahedral Molecules AX_3 and AX_4. *J. Struct. Chem.* **1985**, *26*, 451-475.

(8) Schwerdtfeger, P.; Laakonen, L. J., Pyykkö, P. Trends in inversion barriers. 1. Group-15 hydrides. *J. Chem. Phys.* **1992**, *96*, 6807-6819.

(9) Quantum mechanical tunneling can also contribute to inversion processes, but tunneling is not considered further here; see: Varga, Z.; Verma, P.; Truhlar, D. G. Is the Inversion of Phosphorus Trihalides (PF_3, PCl_3, PBr_3, and PI_3) a Diradical Process? *J. Phys. Chem. A* **2019**, *123*, 301-312.

(10) Montgomery, C. D. Factors Affecting Energy Barriers for Pyramidal Inversion in Amines and Phosphines: A Computational Chemistry Lab Exercise. *J. Chem. Educ.* **2013**, *90*, 661-664.

(11) Bent, H. A. An Appraisal of Valence-Bond Structures and Hybridization in Compounds of the First Row Elements. *Chem. Rev.* **1961**, *61*, 275-311.

(12) Walsh, A. D. The properties of bonds involving carbon. *Discuss Faraday Soc.* **1947**, *2*, 18-25.

(13) Walsh, A. D. The Electronic Orbitals, Shapes and Spectra of Polyatomic Molecules. 4 Tetraatomic Hydride Molecules, AH_3. *J. Chem. Soc.* **1953**, 2296-2301.

(14) Kutzelnigg, W. Chemical Bonding in Higher Main-Group Elements. *Angew. Chem. Int. Ed. Engl.* **1984**, *23*, 272-295.

(15) Related work on transition state structures for S_N2 reactions: Hamlin, T. A.; Swart, M.; Bickelhaupt, F. M. Nucleophilic Substitution (S_N2): Dependence on Nucleophile, Leaving Group, Central Atom, Substituents, and Solvent. *ChemPhysChem* **2018**, *19*, 1315-1330.

(16) Bader, R. F. W. Vibrationally Induced Perturbations in Molecular Electron Distributions. *Can. J. Chem.* **1962**, *40*, 1164-1175.

(17) Pearson, R. G. Concerning Jahn-Teller Effecrts. *Proc. Nat. Acad. Sci. USA* **1975**, *72*, 2104-2106.

(18) Pearson, R. G. The Second Order Jahn-Teller Effect. *J. Mol. Struct.* **1983**, *103*, 25-34.

(19) Levin, C. C. A Qualitative Molecular Orbital Picture of Electronegativity Effects on XH_3 Inversion Barriers. *J. Am. Chem. Soc.* **1975**, *97*, 5649-5655.

(20) Weinhold, F.; Landis, C. R. Valency and Bonding: A Natural Bond Orbital Donor-Acceptor Perspective. Cambridge University Press, 2005, pp. 148-151.

(21) Cherry, W.; Epiotis, N.; Borden, W. T. Effects of Filled π and Unfilled σ Molecular Orbital Interactions on Molecular Structure. *Acc. Chem. Res.* **1979**, *10*, 167-173.

(22) Grev, R. S. Structure and Bonding in the Parent Hydrides and Multiply Bonded Silicon and Germanium Compounds: from MH_4 to $R_2M{=}M'R_2$ and $RM{\equiv}M'R$. *Adv. Organomet. Chem.* **1991**, *33*, 125-170.

(23) Burdett, J. K. Meldola. Medal Lectures I Molecular Shapes. *Chem. Soc. Rev.* **1978**, *7*, 507-520.

(24) Some HOMO-LUMO gaps: https://cccbdb.nist.gov/ (accessed September 2, 2019).

(25) Kira, M. Distortion Modes of Heavy Ethylenes and Their Anions: π–σ^* Orbital Mixing Model. *Organometallics* **2011**, *30*, 4459-4465

(26) Wedler, H.B..; Wendelboe, P.; Power, P. P. Second-Order Jahn-Teller (SOJT) Structural Distortions in Multiply Bonded Higher Main Group Compounds. *Organometallics*, **2018**, *37*, 2829-2936.

(27) Fischer, R. C.; Power, P. P. π-Bonding and the Lone Pair Effect in Multiple Bonds Involving Heavier Main Group Elements. *Chem. Rev.* **2010**, *110*, 3877-3923.

(28) While in many cases the orbital energy gap we investigate is that between the HOMO and the LUMO, in some instances, for symmetry reasons, the gap of interest is between that of the HOMO and the LUMO+1 molecular orbital.

(29) Frisch, M. J.; Trucks, G. W.; Schlegel, H. B.; Scuseria, G. E.; Robb, M. A.; Cheeseman, J. R.; Scalmani, G.; Barone, V.; Mennucci, B.; Petersson, G. A.; Nakatsuji, H.; Caricato, M.; Li, X.; Hratchian, H. P.; Izmaylov, A. F.; Bloino, J.; Zheng, G.; Sonnenberg, J. L.; Hada, M.; Ehara, M.; Toyota, K.; Fukuda, R.; Hasegawa, J.; Ishida, M.; Nakajima, T.; Honda, Y.; Kitao, O.; Nakai, H.; Vreven, T.; Montgomery, J. A.; Peralta, J. E.; Ogliaro, F.; Bearpark, M.; Heyd, J. J.; Brothers, E.; Kudin, K. N.; Staroverov, V. N.; Kobayashi, R.; Normand, J.; Raghavachari, K.; Rendell, A.; Burant, J. C.; Iyengar, S. S.; Tomasi, J.; Cossi, M.; Rega, N.; Millam, J. M.; Klene, M.; Knox, J. E.; Cross, J. B.; Bakken, V.; Adamo, C.; Jaramillo, J.; Gomperts, R.; Stratmann, R. E.; Yazyev, O.; Austin, A. J.; Cammi, R.; Pomelli, C.; Ochterski, J. W.; Martin, R. L.; Morokuma, K.; Zakrzewski, V. G.; Voth, G. A.; Salvador, P.; Dannenberg, J. J.; Dapprich, S.; Daniels, A. D.; Farkas; Foresman, J. B.; Ortiz, J. V.; Cioslowski, J.; Fox, D. J. Gaussian 09, Revision D.02, Wallingford, CT, 2009.

(30) (a) Sengupta, A.; Raghavachari, K. Solving the Density Functional Conundrum: Elimination of Systematic Errors to Derive Accurate Reaction Enthalpies of Complex Organic Reactions. *Org. Lett.* **2017**, *19*, 2576-2589. (b) Weigend, F.; Ahlrichs, R. Balanced Basis Sets of Split Valence, Triple Zeta Valence and Quadruple Zeta Valence Quality for H to Rn: Design and Assessment of Accuracy. *Phys. Chem. Chem. Phys.* **2005**, *7*, 3297-3305.

(31) Scuseria, G. E.; Schaefer, H. F., III. Is coupled cluster singles and doubles (CCSD) more computationally intensive than quadratic configuration-interaction (QCISD)? *J. Chem. Phys.* **1989**, *90*, 3700-3703.

(32) Dunning, T. H., Jr.; Peterson, K. A.; Wilson, A. K. Gaussian Basis Sets for use in Correlated Molecular Calculations. X. The Atoms Aluminum Through Argon Revisited. *J. Chem. Phys.* **2001**, *114*, 9244.

(33) *CYLview*, 1.0b; Legault, C.Y., Universite de Sherbrooke, 2009**,** http://www.cylview.org; (accessed September 11, 2018).

(34) (a) Hanwell, M. D.; Curtis, D. E.; Lonie, D. C.; Vandermeersch, T.; Zurek, E.; Hutchison, G. R. Avogadro: An Advanced Semantic Chemical Editor, Visualization, and Analysis Platform. *J. Chemoinf.* **2012**, *4*, 17. (b) Avogadro: an open-source molecular builder and visualization tool. http://avogadro.cc/ (accessed September 2, 2019).

(35) doi:10.5281/zendo.1202077. matplotlib/matplotlib v2.2.2; Michael Droettboom; Thomas A Caswell; John Hunter; Eric Firing; Jens Hedegaard Nielsen; Antony Lee; Elliott Sales de Andrade; Nelle Varoquaux; David Stansby; Benjamin Root; Phil Elson; Darren Dale; Jae-Joon Lee; Ryan May; Jouni K. Seppänen; Jody Klymak; Damon McDougall; Andrew Straw; Paul Hobson; cgohlke; Tony S Yu; Eric Ma; Adrien F. Vincent; Steven Silvester; Charlie Moad; Jan Katins; Nikita Kniazev; Tim Hoffmann; Federico Ariza; Peter Würtz

(36) Calculations were attempted for BiH_3, but the results were inconsistent and we were unable to fully optimize any structures.

(37) Calculations were attempted for HPbPbH and H_2PbPbH_2, but the results were inconsistent and we were unable to fully optimize any structures.

(38) Jacobsen,H.; Ziegler, T. The Role of Pauli Repulsion in Multiple Bonding: Structural Consequences and Energetic Implications *Comments Inorg. Chem.* **1995**,*17*, 301-317.

(39) Goldberg, D.E.; Harris, D. H.; Lappert, M.F.; Thomas, K.M. A new synthesis of divalent group 4B alkyls $M[CH(SiMe_3)_2]_2$ (M=Ge or Sn), and the crystal and molecular structure of the tin compound. *J. Chem. Soc. Chem. Commun.* **1976**, 261-262.

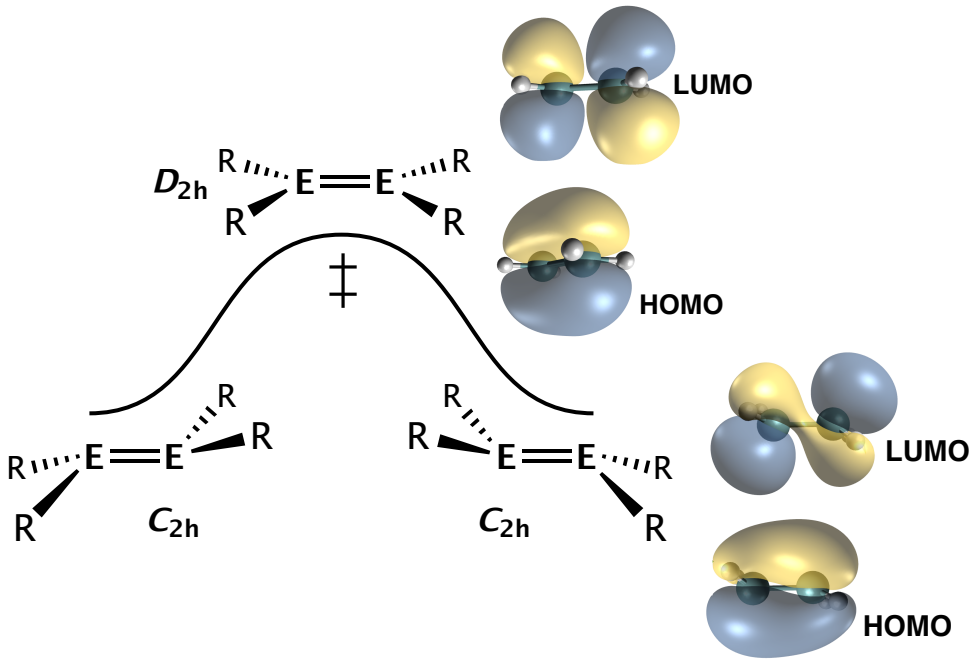

Calculations suggest an upper limit of approximately 12 eV energy separation of the interacting levels for second order Jahn-Teller effects to be significant, which is considerably larger than previously thought.